

Coupled heat and mass transfer in annular adsorption bed

D. D. Gao, Y. X. Li, Z. X. Yuan*, S. W. Du

College of Environmental and Energy Engineering, Beijing University of Technology

Received February 12, 2016; Revised December 26, 2016

A numerical simulation has been conducted to investigate the heat and mass transfer in the adsorption process of an annular cavity bed. The silica gel and the water was taken as the working pair. The 2D model of the heat and mass transfer has been established for the adsorption problem. To clarify the cooling effect of different situations, the air cooling mode and the water cooling mode were considered to apply onto the bed. Based on the numerical results the change of the temperature and the vapor concentration of the bed was analyzed and discussed. The influence of the bed layer porosity and the evaporation temperature on the performance was examined too. The results have revealed that the bed temperature increased largely at the first 400 seconds of the adsorption time. This time corresponded to the rapid adsorption and the large amount of the heat generation. Beyond a summit, the temperature of the bed decreased gradually while the bed concentration kept increasing. The bed layer porosity affected the adsorption only in a small scale, while increasing the evaporation temperature promoted the adsorption largely.

Keywords: adsorption bed, heat and mass transfer, temperature, dynamic

AIMS AND BACKGROUND

Nowadays much attention in the world is being paid to the excessive energy consumption and the environment pollution. Many technologies have been proposed to conserve energy and to reduce the harm to the environment. Specially, utilizing the solar energy as the driving source of the refrigeration system has got the attention of the researchers. Compared to the conventional vapor-compressed refrigeration technique, the adsorption cooling system has the advantage of low grade demanding of the heat source, low noise, and less pollution to the environment [1,2]. Therefore, the related study on such a topic has drawn many researchers around the world [2,3].

In adsorption refrigeration system the adsorbent bed is the most important component. Its characteristic directly affects the performance of the system. Especially, for the solar-driven adsorption system, the performance of the bed is highly affected by the heat and mass transfer in the bed. The solar energy should be transferred into the bed quickly to cause the bed to desorb. On the other hand, the reaction heat in the adsorption process must be discharged out as soon as possible so that the material can fully adsorb the refrigerant vapor. Some measurements have been proposed in the literature to enhance the heat transfer in the bed. Groll reviewed [4] the typical beds in the

adsorption system, he emphasized the same importance of the heat transfer in both the external and the internal sides of the bed. Pons et al studied [5] the dynamic temperature change in the bed and demonstrated the impact of the flow-rate of the circulating fluid. The application of zeolite-active carbon compound in the tube bed could promote the heat transfer by absorbing the solar energy directly [6]. Using the zeolite-coated bed for a sorption air conditioning system, Restuccia et al investigated the optimum conditions to reach the most effective heat and mass transfer [7]. Heat pipes or optimized thermal loops may also improve the performance of a sorption system. A novel design of passive evaporation known as the rising film evaporation was reported in [8], in which the gravity heat pipe was employed to enhance the heat transfer in the evaporator. The author also emphasized the significance of the appropriate arrangement of the thermal fluid and the refrigerant vapor. Niazmand et al [9] conducted a research on the coupling heat and mass transfer in the evacuated tube bed with fins. The numerical results revealed that increasing the fin number and decreasing the bed height was both able to reduce the cycle time.

Considering the intrinsic feature of the coupled heat and mass transfer in the bed, it is necessary to take into account of both them together in the study, so that the mutually-affected mechanism can be clearly verified. For this purpose, the current study is focused on the investigation into the heat and mass transfer in an evacuated tube bed during the

* To whom all correspondence should be sent:

E-mail zxyuan@bjut.edu.cn

adsorption process. The numerical results of the temperature and the adsorption concentration of the bed will be presented and discussed. In addition, the effect of the material porosity and the evaporation temperature will also be paid attention.

PHYSICAL AND MATHEMATICAL MODEL

For simplification, the heat and mass transfer in the evacuated tube bed is reduced to be a 2-D axially symmetrical problem, as shown in Figure 1 and Figure 2. The outer alloy tube and the inner copper tube forms the annular adsorption bed. The silica gel is used as the adsorbent. Through the annular inlet at the left the water vapor flows into the bed. At the same time, the circulating fluid flows through the copper tube to keep the bed cooling down. In the desorption process, which is not involved in this study, the solar irradiation heats the alloy tube through the outmost glass tube. The bed is exposed to the solar radiation and the cooling channel is shut down. Beyond the critical pressure, the desorbed water vapor is delivered to the condenser and liquefied. As the first part of the study, the result here is only for the heat and mass transfer in the adsorption process. The large amount of the reaction heat during the adsorption is rejected by the cooling fluid of either the air or the water. No solar heat is put on the bed during the adsorption process.

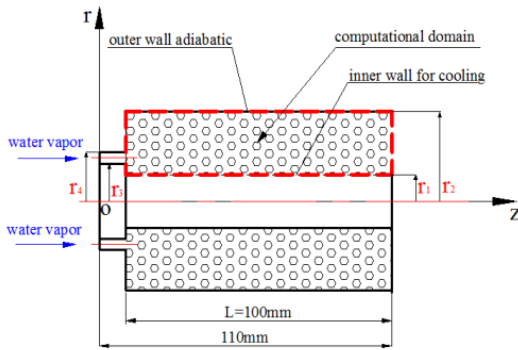


Fig.1. The two-dimensional model of the tube bed

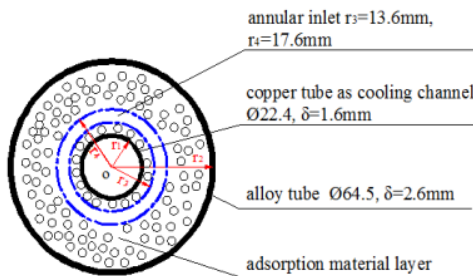


Fig.2. Cross-sectional schematic of the bed

In the numerical model the following assumptions are considered and followed, (a) The adsorbent particle is of the same size. The physical property of the bed material is isotropic, (b) All physical properties are constant and independent of the temperature and the concentration, and (c) The contact resistance between the adsorbent and the tube wall is neglected.

Energy Equation

In the energy equation the balance of the transient source term, the heat conduction, and the vapor convection are involved. The adsorption concentration q of the bed is taken as a heat source term [10]. The energy equation of the adsorption bed is as

$$\begin{aligned} (1-\varepsilon_i)\rho_s c_{ps} + \varepsilon_b \rho_g c_{pg} + (1-\varepsilon_i)\rho_s q c_{pw} \frac{\partial T_s}{\partial t} = \lambda_{\text{eff}} \left[\frac{1}{r} \frac{\partial}{\partial r} \left(r \frac{\partial T_s}{\partial r} \right) + \frac{\partial^2 T_s}{\partial z^2} \right] \\ - \frac{\partial}{\partial z} (\rho_g c_{pg} T_s u) + (1-\varepsilon_i)\rho_s \Delta H_{\text{ads}} \frac{\partial q}{\partial t} \end{aligned} \quad (1)$$

where, c_{ps} and c_{pg} is the specific heat of the adsorbent material and the refrigerant vapor, respectively. c_{pw} is the specific heat of the liquid refrigerant. u indicates the flowing velocity of the refrigerant vapor in the bed. λ_{eff} is the effective heat conductivity, which was determined by the weighted sum of the adsorbent's and the vapor's conductivity. ΔH_{ads} is the reaction heat of adsorption. The total porosity of the bed ε_i is determined by the weighted sum of the bed layer porosity ε_b and the particle porosity ε_p ,

$$\varepsilon_i = \varepsilon_b + (1-\varepsilon_b)\varepsilon_p \quad (2)$$

The boundary condition for the energy equation is

$$r = r_1, \quad -\lambda_{\text{eff}} \frac{\partial T(r, z)}{\partial r} \Big|_w = h(T_w - T_f) \quad (3)$$

$$r = r_2, \quad -\lambda_{\text{eff}} \frac{\partial T(r, z)}{\partial r} \Big|_w = 0 \quad (4)$$

$$r_1 < r < r_2, \quad \frac{\partial T_s}{\partial z} \Big|_{z=10} = \frac{\partial T_s}{\partial z} \Big|_{z=110} = 0 \quad (5)$$

Where h is the convective heat transfer coefficient between the coolant fluid and tube wall. Both the air and the water are taken as the coolant fluid. By the reference of the heat transfer handbook, we took $h = 6 \text{ W}/(\text{m}^2 \cdot \text{K})$ for the natural air convection, and $h = 500 \text{ W}/(\text{m}^2 \cdot \text{K})$ for the forced water convection. These two thermal boundary conditions will be the basis of the following comparison for the different cooling situation. In addition, the initial condition of the bed in the simulation is considered as

$$T(r, z, t) \Big|_{t=0} = 298 \text{ (K)} \quad (6)$$

The property of the type-A silica gel was adopted in the simulation. The diameter of the silica gel particle was taken as $d = 1.0\text{mm}$. The other properties of the silica gel are listed in Table 1.

Mass Equation

The mass equation describes the transient equivalence between the vapor convection and the vapor mass change in the pores of the bed

$$\frac{\partial(\varepsilon_t \rho_g)}{\partial t} + \nabla(\rho_g \bar{u}) = S_m \quad (7)$$

The source term S_m reflects the change of the adsorption concentration per unit time. It takes a negative value in the adsorption process and a positive value in the desorption process. The S_m term can be determined directly by the change of the concentration with the time

$$S_m = -(1 - \varepsilon_t) \rho_s \frac{\partial q}{\partial t} \quad (8)$$

Velocity Equation

For the hydrodynamic problem in a porous media where the effective porosity is not very high, the Darcy's law of the hydromechanics is applied. The Darcy's law describes the relation of the fluid velocity and the pressure gradient. Provided that the viscosity of the fluid μ and the apparent permeability K_{app} of the material is known, the velocity u has the relation to the pressure p as

$$u = -\frac{K_{app}}{\mu} \frac{\partial p}{\partial z} \quad (9)$$

The corresponding boundary condition for the current problem is

$$\left. \frac{\partial p}{\partial z} \right|_{z=110} = 0$$

$$p|_{z=10} = p_e \quad (10)$$

The initial pressure of the bed is assumed as $p = 0$.

The apparent permeability K_{app} is related to the intrinsic permeability of the material K and the physical property of the fluid [11,12]

$$K_{app} = K + \frac{\varepsilon_p \mu}{\tau p} D_g \quad (11)$$

Where τ is the collision factor and D_g is the diffusivity of the fluid. According to the theory of the transport phenomena, K is determined by the particle size d and the bed layer porosity ε_b , and is calculated by the semi-empirical Blake-Kozeny formula

$$K = \frac{\varepsilon_b^3 d^2}{150(1 - \varepsilon_b)^2} \quad (12)$$

The diffusivity D_g of the refrigerant vapor in

Eq.(11) is determined by the formula [13,14]

$$D_g = 1/(1/D_m + 1/D_k) \quad (13)$$

where D_m and D_k is the molecular diffusivity and the Knudsen diffusivity respectively

$$D_m = 0.02628 \frac{\sqrt{T^3/M}}{p\sigma^2\Omega} \quad (14)$$

$$D_k = \frac{2 \times 10^5 r_p}{3} \left(\frac{8RT}{\pi M} \right)^{1/2} \quad (15)$$

In Eq.(14) and (15), M is the molecular mass of the vapor. R is the universal ideal gas constant. σ is the collision diameter for the Lennard-Jones potential, and Ω is the collision integral. r_p denotes the radius of the adsorbent particle.

Adsorption Equation

The current adsorption problem is a typical non-equilibrium process. Based on the reaction kinetics theory, Sakoda and Suzuki studied the adsorption dynamics in the silica gel-water system. They argued that the adsorption rate was strongly influenced by the surface diffusion of the adsorbent particle [15]. To reflect the feature of the actual non-equilibrium in the adsorption process, they took into account the effect of the surface diffusion into the adsorption rate, and proposed the dynamic model as

$$\frac{\partial q}{\partial t} = \frac{15D_{so} \exp(-E_a/RT)}{r_p^2} (q^* - q) \quad (16)$$

The initial condition is $q = 0$ for $t = 0$, and D_{so} is the surface diffusivity of the material. q^* is the equilibrium concentration that is determined by the modified Dubinin-Astakhov equation

$$q^* = k(p_e/p_s)^{\frac{1}{n}} \quad (17)$$

k and n are constants related to the working pair. For the silica gel - water system, $k = 0.346 \text{ g}_w/\text{g}_s$ and $n = 1.6$. p_e is the evaporation pressure, and p_s is the saturation vapor pressure corresponding to the bed temperature T_s . In the numerical simulation, we adopted the empirical Antoine formula to determine the relationship of the saturation pressure and the temperature of water [16,17]

$$\lg p = A - B/(T + C) \quad (18)$$

$A = 8.10765$, $B = 1750.29$, $C = 235$, for $T = 0 \sim 60 \text{ }^\circ\text{C}$, and $A = 7.96681$, $B = 1668.21$, $C = 228$, for $T = 60 \sim 150 \text{ }^\circ\text{C}$.

It needs to note that the unit of the pressure in Eq.(18) is in mmHg.

Table 1. Physical properties of type A silica gel[10].

Average pore size (nm)	Specific surface (m ² /g)	Pore volume (ml/g)	Specific heat c_{ps} (kJ/(kg·K))	Thermal conductivity λ_s (W/(m·K))	Bulk density ρ_s (kg/m ³)	True density (kg/m ³)	Apparent density (/kg/m ³)
2.0-3.0	650-800	0.35-0.45	0.92	0.175	790	2200	1170

Table 2. The parameter values for the numerical model

Parameter	Symbol	Value	Unit
Initial inlet pressure	p_0	1703.5	Pa
Surface diffusion coefficient	D_{so}	2.54×10^{-4}	m ² /s
Activation energy of surface diffusion [18]	E_a	4.2×10^4	J/mol
Universal gas constant ¹⁸	R	8.314	J/(mol·K)
Specific gas constant for water vapor	R_g	461.5	J/(kg·K)
Adsorption heat of silica gel [13]	ΔH_{ads}	2560	kJ/kg
Particle density of silica gel	ρ_s	790	kg/m ³
Thermal conductivity of silica gel	λ_s	0.175	W/(m·K)
Specific heats of silica gel	c_{ps}	0.920	kJ/(kg·K)
Particle porosity of silica gel [10]	ϵ_p	0.42	—
Bed porosity [10]	ϵ_b	0.37	—
Specific heat of water vapor	c_{pg}	1.874	kJ/(kg·K)
Specific heat of water	c_{pw}	4.187	kJ/(kg·K)
Molecular weight of water	M	18	g/mol
Viscosity of water vapor	μ	9.06×10^{-6}	N·s/m ²
Thermal conductivity of water vapor [19]	λ_g	0.0196	W/(m·K)
Collision factor [13]	τ	3	—
Collision diameter for Lennard-Jones potential [13]	σ	2.641	Å
Collision integral [12]	Ω	2.236	—
Evaporation temperature	T_e	288	K

Table 3. Converged temperature of the monitored points for different grid system, water cooling condition at $T_f = 298K$, $h = 500 W/(m^2 \cdot K)$

Grid number	T_A (K)	T_C (K)	T_D (K)
14500	307.69	308.04	318.31
25737	307.38	307.64	318.30
57500	307.30	307.67	318.23
103193	307.44	307.83	318.25

NUMERICAL METHOD

The numerical simulation to the current problem was conducted by using the FLUENT software. The GAMGIT program involved in the software package was used to generate the grid system. In advance of the simulation, the parameters that are involved in the equations above must be preset. By reference of the open literature that was related to the dynamic adsorption problem, the corresponding parameters were adopted and listed in Table 2.

In a simulation it is necessary to check the grid-independence of the numerical domain prior to the formal calculation. The appropriate grid system guarantees the convergence of the iteration and the accuracy of the numerical result. For this purpose, a preliminary study was conducted for the water cooling case. In the process of the iteration the

temperature, the pressure and the adsorption concentration of the bed were monitored. The monitored points are denoted by A, B, C, and D as shown in Figure 3, which coordinator value is as A(30, 15.6), B(50, 15.6), C(70, 15.6) and D(50, 27.6) respectively.

In the preliminary simulation, the temperature of point A, C and D was monitored for the different grid system. The checked result is presented in Table 3. With the grid number increasing from 14500 to 103193, the temperature changed not very much. The changing range of the temperature was in between 0.08K and 0.40K, with the maximum for point C and the minimum for point D. Therefore it was considered that the grid number in the range above did not affect the numerical accuracy too much, and then the grid number of 25737 was adopted in the formal study.

Table 4. Relation of the evaporation temperature to the pressure.

T (°C)	5	8	12	15
p_s (Pa)	871.5	1072.1	1401.5	1703.5

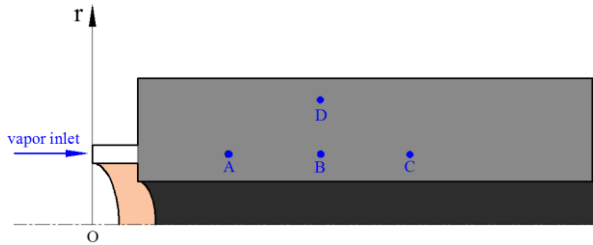


Fig.3. The numerical domain and the monitored points position.

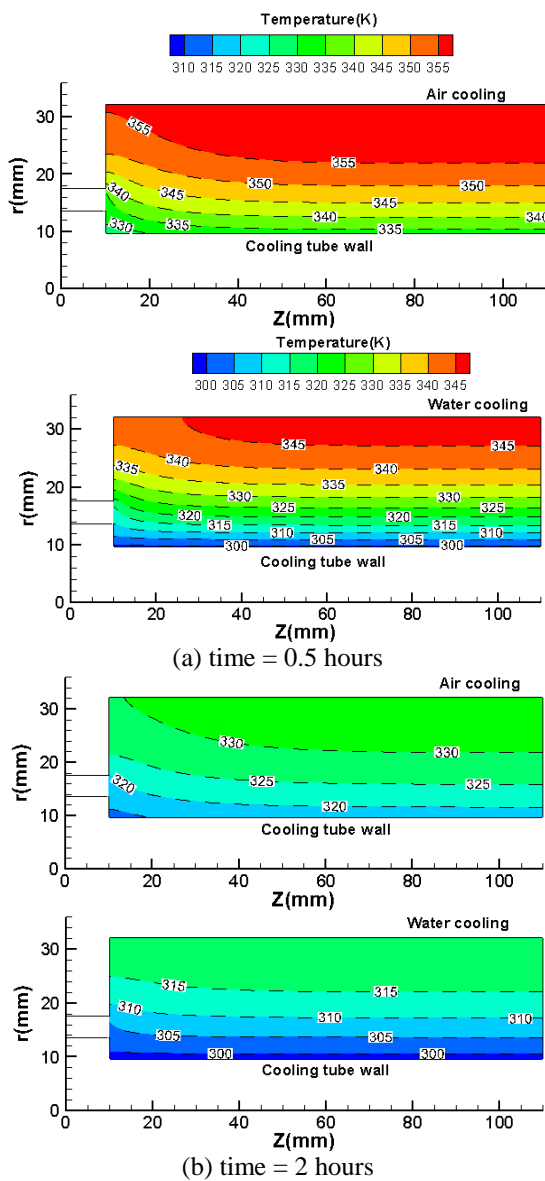


Fig. 4. Comparison of the temperature field for the air cooling and the water cooling, as adsorption time was 0.5 hour and 2 hours, respectively.

RESULTS AND DISCUSSION

Temperature and Concentration Field

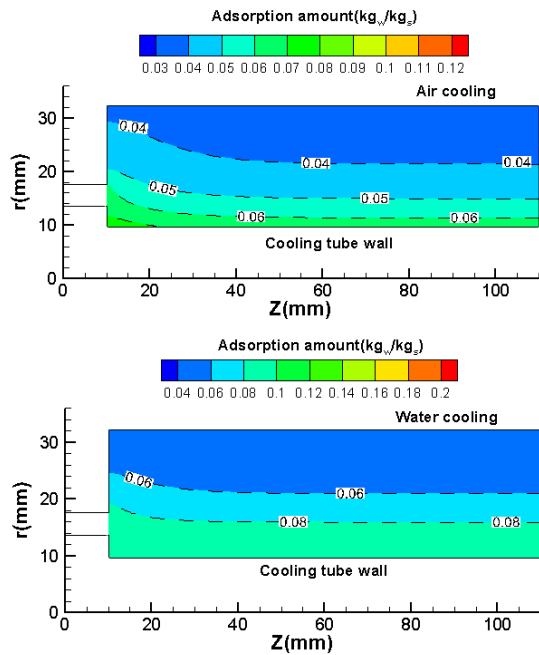
To analyze the distribution of the temperature, two sets of the temperature field of the bed at different time were presented in Figure 4. Figure 4 (a) and (b) is for the $t = 0.5$ hours and for the $t = 2$ hours of the adsorption time respectively. Obviously, the bed temperature distributed much more evenly at $t = 2$ hours as compared to that at time = 0.5 hours. After one and a half hours adsorption, the non-uniformity degree of the temperature had decreased from 25K to 15K for the air cooling, and from 45K to 15K for the water cooling. It is seen from the figure that the temperature changes more seriously along the radial direction rather than the axial direction. This tells us that the heat transfer was mainly towards the radial direction. As to the effect of the cooling mode, the cold area reflects the difference. In comparison, the cold area of the water-cooling patterns is clearly larger than that of the air cooling patterns. This demonstrates that the water cooling mode is better than the air cooling mode. The cooling effectiveness of the bed is very important in view of the sufficient adsorption of the material. The lower temperature promotes the adsorption while the high temperature frustrates the adsorption.

The corresponding concentration field to the above temperature field is shown in Figure 5. Different from the less-changing temperature field with the time, here the gradient of the concentration became greater with the time as comparing Figure 5 (b) to Figure 5 (a). This just reflected the effect of the temperature on the adsorption process. The inner cold area of the bed near the cooling tube wall tended to adsorb more strongly than the outer area. On the other hand, the adsorption difference resulted from the cooling mode is obvious. The high cooling strength of the water helped to improve the adsorption in the bed. Though the isosteric values in Figure 5(a) was not very different for the air cooling mode and for the water cooling mode, their difference in Figure 5(b) was as great as almost two times. The water cooling mode had the great advantage and should be taken into account in practical engineering.

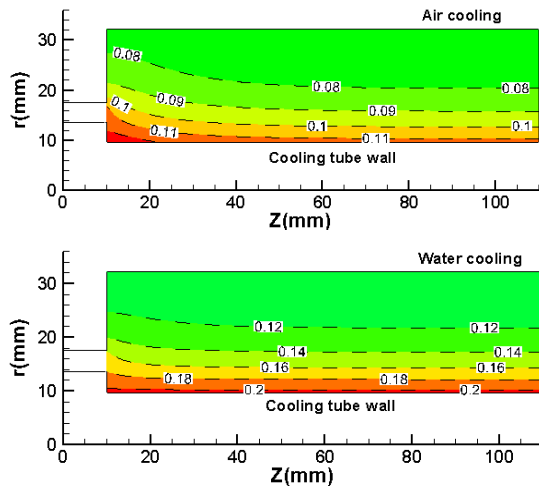
Dynamic Change of Temperature and Concentration

On the basis of the distribution field discussed above, it is necessary to delve into the temporal evolution of the temperature in the bed. In Figure 3 four points A, B, C, and D were taken to monitor

the change of the bed parameters. The dynamic response of the temperature and the concentration of the monitored points are shown in Figure 6 and Figure 7.



(a) time = 0.5 hours



(b) time = 2 hours

Fig. 5. Comparison of the concentration field for the air cooling and the water cooling mode, as adsorption time was 0.5 hour and 2 hours, respectively.

The temperature summit in Figure 6 is considered to be resulted from the unmatched heat dispersion between the adsorption heat generation and the poor capability of the conductivity of the adsorbent material. The large amount of reaction heat resulted from the adsorption at the beginning period could not be transferred effectively by the bed and then caused the sharply rising of the temperature. To distinguish the temperature difference of the monitored points,

a local enlarged view has been inserted into Figure 6. It is clear that the temperature curve of point D was different from the others. With the farthest distance to the cooling tube wall, the point D was of the greater thermal resistance. Therefore point D was subjected to the poorest cooling effect among the monitored points. The maximum temperature difference between point D and the others has reached 28K. The difference between the other three points was much less. A careful survey to the enlarged view revealed that the temperature of point A was the lowest.

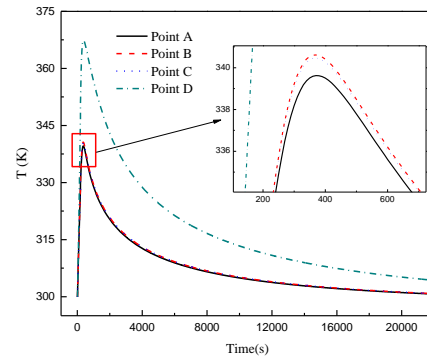


Fig.6. Dynamic change of the temperature of the monitored points for water cooling mode

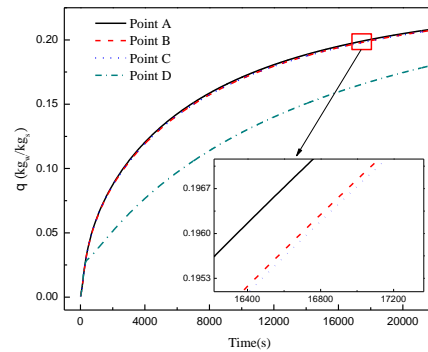


Fig. 7. Dynamic change of the concentration of the monitored points for water cooling mode

The change of the concentration is presented in Figure 7. After a rapid increasing at the beginning time, the adsorption rate tended to slow down gradually. A feature needs to pay attention is the sharp turning of the curve of point D. Approximately at time = 300 s, the adsorption rate of point D dropped down suddenly, and then the curve began to separate from the others. This feature can be interpreted from the relationship of the heat transfer ability and the mass transfer ability of the material. With higher diffusivity of the material than the conductivity, all points got a chance to adsorb quickly at the beginning. But with the proceeding of the adsorption, the inferior position of point D occurred right away because of the poor heat dissipation to the coolant fluid. The

bad cooling effect of point D frustrated its effective adsorption further more. As to point A, B, and C, not much difference was detected because they all share the same radial coordinate value.

Effect of Cooling Mode on Bed Performance

Different cooling conditions will result in the different performance of the bed. With the air cooling mode and the water cooling mode, the numerical simulation has presented the variation of the bulk average temperature and the average adsorption concentration of the bed, as shown in Figure 8 and Figure 9.

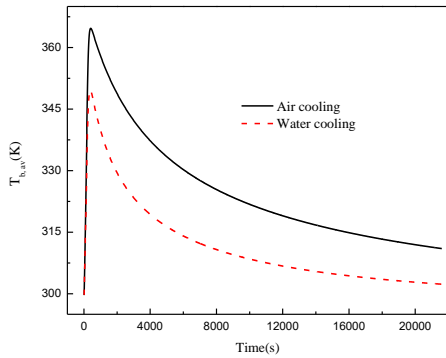


Fig. 8. Variation of the average temperature with the time.

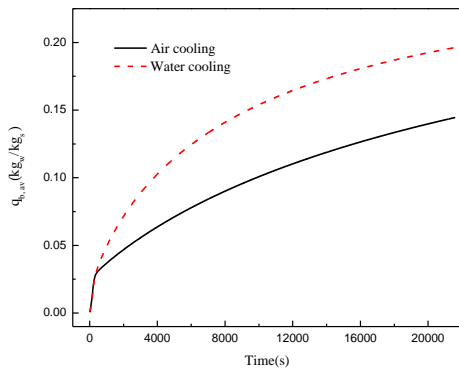


Fig. 9. Variation of the average concentration with the time.

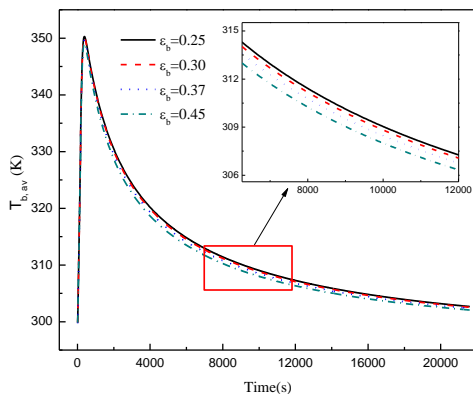


Fig.10. Porosity effect on the temperature change of the bed, for water cooling mode.

The variation of the bulk average temperature is similar to that of the monitored point in Figure 6. In Figure 8 the average temperature reached the maximum of 364.7K after 410s for the air cooling condition, and 349.6K after 380s for water cooling condition. The difference of the dynamic temperature for the two cooling modes is obviously. With less difference before the summit, the average temperature of the bed for the water cooling mode decreased faster than that of the air cooling mode. The maximum difference of the temperature for them was as much as 19.3K.

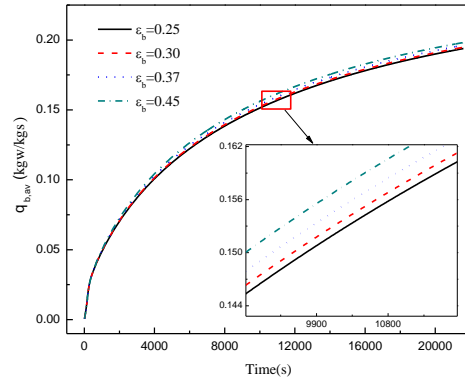


Fig. 11. Porosity effect on the concentration change of the bed, for water cooling mode.

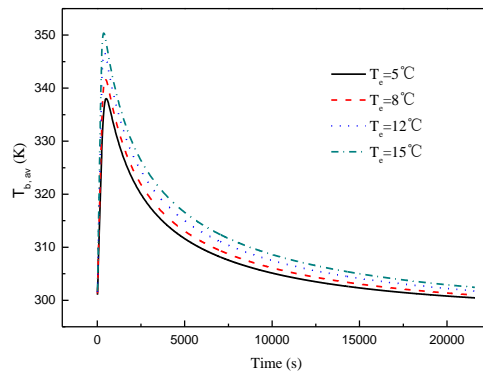


Fig. 12. Effect of the evaporation temperature on the bed temperature, for water cooling mode.

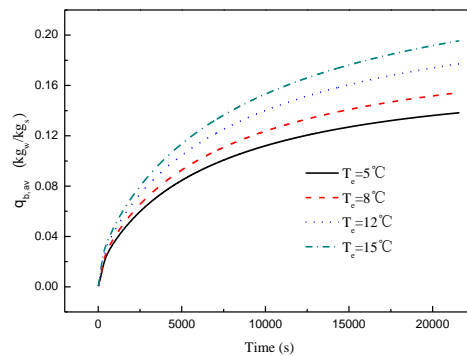


Fig.13. Effect of the evaporation temperature on the average concentration of the bed, for water cooling mode.

The bulk averaged concentration of the bed is presented in Figure 9. The figure shows the different tendency of the average concentration for the two cooling modes. The water cooling mode generates a smoothly increasing profile of the $q_{b,av}$, while the increasing of the concentration of the air cooling mode slowed down after a time period. The maximum difference of the concentration for the two cooling modes has reached 26.4%. The causation of this phenomenon is similar to what is mentioned in the discussion of Figure 7. After the transient effective adsorption at the beginning time, the good cooling way of the water mode tended to keep the bed in a sustainable good work state, while the air cooling mode does not have such ability because of the less cooling effect. Usually the power output of the refrigeration machine depends mainly on the adsorption amount per unit time, so the appropriate cooling way is highly appreciated.

Effect of Porosity of Adsorbent on Bed Performance

As aforementioned the total porosity of the bed consists of the particle porosity ε_p and the bed layer porosity ε_b . The ε_p is an intrinsic attribute of the adsorption material, which is determined by the product type, but the ε_b is changeable with the compactness of the bed. Leong et al [20] once conducted a study of the compressing effect of the adsorbent particle on the heat and mass transfer of the bed. Their result suggested that although the compacted bed improved the heat transfer, the decreased bed porosity affected the adsorption inversely. With the bed porosity decreasing, the mass transfer resistance increased, which would hinder the adsorption of the bed.

In the current study the bed porosity ε_b was considered as a variable. In the range of ε_b from 0.25 to 0.45, the effect of the bed porosity was numerically identified. The related variation of the $T_{b,av}$ and $q_{b,av}$ with the time is as shown in Figure 10 and Figure 11. It is seen that the effect of the bed porosity on the performance is not seriously. The maximum temperature difference for the different porosities was only about 1.8K, and the maximum concentration difference was about 2.2%. In addition, the result of the porosity effect was consistent with the conclusion of the study by Leong et al in [20]. The higher porosity did lower the average temperature of the bed to some extent, and promoted the adsorption slightly.

Effect of Evaporation Temperature on Bed Performance

The pressure of the refrigerant vapor is another significant factor to influence the adsorption. The

equilibrium concentration of the adsorbent material usually increases with the pressure and decreases with the temperature. On the other hand, the influence of the two elements is not in the same level. In the current study, a series of simulation has been performed on the effect of the inlet pressure of the refrigerant vapor. The numerical condition was the same as presented in Table 2 with the water cooling mode. Four pressure values were adopted, and their relation to the evaporation temperature is as shown in Table 4. The p_s is the saturation pressure at the given temperature. Figure 12 presented the change of the bed temperature $T_{b,av}$ at different evaporation temperatures. As seen in the figure, the bed temperature increased largely with the evaporation temperature. Increasing the evaporation temperature implies improving the inlet pressure of the vapor into the bed. The higher pressure upgraded the driving force of the adsorption. The improved adsorption generated more reaction heat and resulted in the temperature rising up quickly.

The effect of the evaporation temperature on the bed concentration is presented in Figure 13. Obviously, the evaporation temperature affected the bed concentration more strongly than the bed porosity, as shown in Figure 11. The maximum difference of the $q_{b,av}$ for $T_e = 5^\circ\text{C}$ and 15°C has reached as much as 67.7%. If we relate the $q_{b,av}$ curve to the $T_{b,av}$ curve in Figure 12, an interesting relationship is revealed. Corresponding to the shooting up of the temperature curve at the beginning time, the concentration curve increased fast too. To the declining temperature beyond the summit, the concentration curve tended to be flat. The higher temperature profile corresponded to the higher concentration profile. This feature is just the reverse to the relation of the $T_{b,av}$ and the $q_{b,av}$ discussed above about the effect of the cooling mode and the bed porosity. The high temperature of the bed itself frustrated the adsorption, while the high temperature of the evaporator helped to promote the adsorption. This reflects the difference of the adsorption driving potential from the outside and the inside of the adsorbent particle.

CONCLUSIONS

Based on the established model of the annular bed, the numerical simulation was performed on the characteristics of the adsorption process. The results revealed that the heat and mass transfer in the bed was highly coupled and affected each other. The temperature distribution of the bed was the integrated result of the adsorption and the cooling mode. The bed temperature also reacts against the

adsorption strongly. For the annular bed with the internal cooling tube, the water cooling mode resulted in a much better adsorption performance than the air cooling mode. At the beginning time the adsorption happened in a high rate, and a large amount of the reaction heat was generated. The heat generation resulted in a rapid rise of the temperature within the first 400 seconds or so. After reaching the summit, the bed temperature declined gradually. Correspondingly, the adsorption experienced a process from fast to slowing down.

Further study revealed that the higher bed porosity tended to reduce the mass transfer resistance and to improve the adsorption slightly. On the other hand, increasing the inlet vapor pressure of the bed promoted the adsorption in large scale. In general, applying the effective cooling mode, optimizing the bed structure, and reducing the heat and mass transfer resistance, are considered as the effective ways to improve the performance of the adsorption bed.

NOMENCLATURE

c_{ps}	[J/(kg·K)]	specific heat of silica gel
c_{pg}	[J/(kg·K)]	specific heat of refrigerant vapor
c_{pw}	[J/(kg·K)]	specific heat of refrigerant liquid
d	[m]	particle diameter
D_g	[m ² /s]	diffusivity of refrigerant vapor
D_k	[m ² /s]	Knudsen diffusivity of the material
D_m	[m ² /s]	molecular diffusivity of the material
D_{so}	[m ² /s]	surface diffusion coefficient
E_a	[J/mol]	diffusional activation energy
h	[W/(m ² ·K)]	convective heat transfer coefficient
K	[m ²]	intrinsic permeability of porous material
K_{app}	[m ²]	apparent permeability of porous material
k	[-]	constant in Eq.(17)
M	[g/mol]	molecular mass
n	[-]	constant in Eq.(17)
p	[Pa]	pressure
$p_{b,av}$	[Pa]	average pressure of adsorbent bed
p_s	[Pa]	saturated vapor pressure
q	[kg _w /kg _s]	adsorption concentration
q^*	[kg _w /kg _s]	equilibrium adsorption concentration
$q_{b,av}$	[kg _w /kg _s]	average adsorption capacity of bed
R	[J/(mol·K)]	universal ideal gas constant
r	[mm]	radial coordination
r_1	[mm]	radius of the cooling tube
r_2	[mm]	radius of the solar-absorbing alloy tube
r_p	[m]	radius of adsorbent particle
S_m	[kg/(m ³ ·s)]	mass source term in Eq.(7)
T	[K]	temperature
$T_{b,av}$	[K]	average temperature of adsorbent bed
T_e	[K]	evaporation temperature
T_f	[K]	temperature of the cooling fluid
T_s	[K]	temperature of the adsorbent
T_w	[K]	wall temperature of the cooling tube
T_0	[K]	initial temperature of the bed
t	[s]	time
u	[m/s]	velocity
Greek symbol		
μ	[N·s/m ²]	dynamic viscosity
ρ_g	[kg/m ³]	density of water vapor
ρ_s	[kg/m ³]	density of adsorbent
ΔH_{ads}	[kJ/kg]	heat generation of adsorption
ε_b	[-]	bed layer porosity
ε_p	[-]	particle porosity
ε_t	[-]	total porosity
τ	[-]	collision factor
σ	[Å]	collision diameter for Lennard-Jones potential
Ω	[-]	collision integral
λ_{eff}	[W/(m·K)]	effective thermal conductivity
λ_g	[W/(m·K)]	thermal conductivity of water vapor
λ_s	[W/(m·K)]	thermal conductivity of adsorbent

Acknowledgements: This research work was sponsored by the National Natural Science Foundation of China (Grant No. 51276005) and the National Key Basic Research Program of China (No.2015CB251303).

REFERENCES

1. W. Gazda, J. Koziol, *Appl. Energy*, **101**, 49 (2013).
2. H.Z. Hassan, A.A. Mohamad, R. Bennacer, *Energy*, **36**, 530 (2011).
3. R.Z. Wang, *Renewable Sustainable Energy Rev*, **5**, 1 (2001).
4. M. Groll, *Heat Recovery Syst. CHP*, **13**, 341 (1993).
5. M. Pons, D. Laurent, F. Meunier, *Appl. Therm Eng*, **16**, 395 (1996).
6. Z.Y. Liu, Y.Z. Lu, J.X. Zhao, *Sol. Energy Mater. Sol. Cells*, **52**, 45 (1998).
7. G. Restuccia, A. Freni, G. Maggio, *Appl. Therm. Eng*, **22**, 619 (2002).
8. R.Z. Wang, Z.Z. Xia, L.W. Wang, Z.S. Lu, S.L. Li, T.X. Li, J.Y. Wu, S. He, *Energy*, **36**, 5425 (2011).
9. H. Niazmand, I. Dabzadeh, *Int. J. Refrig*, **35**, 581 (2012).
10. H.T. Chua, K.C. Ng, W. Wang, C. Yap, X.L. Wang, *Int. J. of Heat Mass Transfer*, **47**, 659 (2004).
11. K.C. Leong, Y. Liu, *Int. J. of Heat Mass Transfer*, **47**, 4761 (2004).
12. R.B. Bird, W.E. Stewart, E.N. Lightfoot, *Transport Phenomena*, Wiley, New York, 1960.
13. H. Demir, M. Mobedi, S. Ülkü, *Int Commun Heat Mass Transfer*, **36**, 372 (2009).
14. D.M. Ruthven, *Principles of adsorption and adsorption processes*, John Wiley & Sons, New York, 1984, p. 124
15. A. Sakoda, M. Suzuki, *J. Chem. Eng. Jpn*, **17**, 52 (1984).
16. R.C. Reid, J.M. Prausnitz, T.K. Sherwood, *The properties of gases and liquids*, fourth ed., McGraw-Hill, New York, 1987.
17. A. Senol, *J. Chem. Thermodyn*, **67**, 28 (2013).
18. J. Di, J.Y. Wu, Z.Z. Xia, R.Z. Wang, *Theoretical Int. J. Refrig*, **30**, 515 (2007).
19. İ. Solmuş, D. Andrew, S. Rees, C. Yamali, D. Baker, B. Kaftanoğlu, *Int. J. Refrig*, **35**, 652 (2012).
20. K.C. Leong, Y. Liu, *Appl. Therm. Eng*, **24**, 2359(2004).